The Journal of Immunology

CD73 Inhibition Shifts Cardiac Macrophage Polarization toward a Microbicidal Phenotype and Ameliorates the Outcome of Experimental Chagas Cardiomyopathy

Nicolás Eric Ponce, Liliana Maria Sanmarco, Natalia Eberhardt, Mónica Cristina García, Héctor Walter Rivarola, Roxana Carolina Cano and Maria Pilar Aoki

J Immunol published online 22 June 2016
http://www.jimmunol.org/content/early/2016/06/22/jimmunol.1600371

The Journal of Immunology is published twice each month by The American Association of Immunologists, Inc., 9650 Rockville Pike, Bethesda, MD 20814-3994.

Print ISSN: 0022-1767 Online ISSN: 1550-6606.

Published June 22, 2016, doi:10.4049/jimmunol.1600371

CD73 Inhibition Shifts Cardiac Macrophage Polarization toward a Microbicidal Phenotype and Ameliorates the Outcome of Experimental Chagas Cardiomyopathy

Nicolás Eric Ponce,* Liliana Maria Sanmarco,* Natalia Eberhardt,* Mónica Cristina García,† Héctor Walter Rivarola,‡ Roxana Carolina Cano,*,§ and Maria Pilar Aoki*

Increasing evidence demonstrates that generation of extracellular adenosine from ATP, which is hydrolyzed by the CD39/CD73 enzyme pair, attenuates the inflammatory response and deactivates macrophage antimicrobial mechanisms. Although CD73 is emerging as a critical pathway and therapeutic target in cardiovascular disorders, the involvement of this ectonucleotidase during myocardial infection has not been explored. Using a murine model of infection with *Trypanosoma cruzi*, the causal agent of Chagas cardiomyopathy, we observed a sudden switch from the classical M1 macrophage (microbicidal) phenotype toward an alternative M2 (repairing/anti-inflammatory) phenotype that occurred within the myocardium very shortly after BALB/c mice infection. The observed shift in M1/M2 rate correlated with the cardiac cytokine milieu. Considering that parasite persistence within myocardium is a necessary and sufficient condition for the development of the chronic myocarditis, we hypothesized that CD73 activity may counteract cardiac macrophage microbicidal polarization, rendering the local immune response less effective. In fact, a transient treatment with a specific CD73 inhibitor (adenosine 5′-α,β-methylene-diphosphate) enhanced the microbicidal M1 subset predominance, diminished IL-4– and IL-10–producing CD4$^+$ T cells, promoted a proinflammatory cytokine milieu, and reduced parasite load within the myocardium during the acute phase. As a direct consequence of these events, there was a reduction in serum levels of creatine kinase muscle–brain isoenzyme, a myocardial-specific injury marker, and an improvement in the electrocardiographic characteristics during the chronic phase. Our results demonstrate that this purinergic system drives the myocardial immune response postinfection and harbors a promising potential as a therapeutic target. ***The Journal of Immunology*****, 2016, 197: 000–000.**

Chagas disease is caused by *Trypanosoma cruzi* infection and constitutes a major public health problem in Latin America due to its prevalence, morbidity, and mortality. About 7 million people are estimated to be infected worldwide, mostly in Latin American countries, but the disease has been spread to nonendemic regions, and thousands of new cases are diagnosed each year (1). Because the cardiomyopathy represents the most frequent and serious complication of Chagas disease, affecting ∼30–40% of infected individuals, chagasic myocarditis is the most common form of nonischemic cardiomyopathy worldwide. During the acute phase, the parasites replicate in tissues throughout the body, showing a strong tropism for the myocardium. Innate and adaptive immune responses control the parasite levels, but are insufficient to completely clear the infection, and most individuals remain infected for life. The myocardial parasite persistence is central for the etiology of the cardiomyopathy (2, 3). Although, it has been recognized that host resistance to *T. cruzi* infection is exerted mainly by cell-mediated reactions involving specific T lymphocytes and macrophages (Ma) (4), the mechanisms by which the Ma-protective response fails to eliminate the parasite are not well understood.

Ma represent the first line of defense against pathogens and orchestrate tissue repair mechanisms to preserve or restore homeostasis. To accomplish these roles, they are highly plastic and can adapt to environmental stimuli, displaying either a classically activated (M1) or alternatively activated (M2) profile, which represent extremes of a spectrum of functional phenotypes (5). M1 Ma are classically activated by proinflammatory Th1 cytokines (IFN-γ and IL-12) and LPS. Besides being APCs, the M1 subset shows an enhanced microbicidal capacity attributable to the production of free radicals (such as hydrogen peroxide, superoxide, NO, and peroxynitrite) and inflammatory cytokines (TNF, IL-1β, IL-6, IL-12, and IL-23). On the other extreme, M2 Ma are alternatively activated by Th2 cytokines (IL-4 and IL-13) or by anti-inflammatory mediators (IL-10),

*Departamento de Bioquímica Clínica, Facultad de Ciencias Químicas, Centro de Investigaciones en Bioquímica Clínica e Inmunología–Consejo Nacional de Investigaciones Científicas y Técnicas, Universidad Nacional de Córdoba, Córdoba 5000, Argentina; †Departamento de Farmacia, Facultad de Ciencias Químicas, Unidad de Investigación y Desarrollo en Tecnología Farmacéutica–Consejo Nacional de Investigaciones Científicas y Técnicas, Universidad Nacional de Córdoba, Córdoba 5000, Argentina; ‡Facultad de Ciencias Médicas, Centro de Estudios e Investigación de la Enfermedad de Chagas y Leishmaniasis, Universidad Nacional de Córdoba, Córdoba 5000, Argentina; and §Facultad de Ciencias Químicas, UA Área de Ciencias Agrarias, Ingeniería, Ciencias Biológicas y de la salud–Consejo Nacional de Investigaciones Científicas y Técnicas, Universidad Católica de Córdoba, Córdoba 5000, Argentina

ORCIDs: 0000-0002-7052-5086 (N.E.P.); 0000-0002-2075-8826 (L.M.S.); 0000-0002-6897-7702 (M.P.A.).

Received for publication March 3, 2016. Accepted for publication May 26, 2016.

This work was supported by grants from the Agencia Nacional de Promoción Científica y Tecnológica–Fondo para la investigación Científica y Tecnológica (FONCyT) (PICT 2013-2885), Consejo Nacional de Investigaciones Científicas y Técnicas (CONICET) de la República Argentina (PIP 11220120100620 CO); Secretaría de Ciencia y Tecnología–Universidad Nacional de Córdoba (103/15), and Ministerio de Ciencia y Tecnología de la Provincia de Córdoba (1143/10). N.E.P. was supported by a CONICET postdoctoral scholarship. L.M.S. and M.C.G. were supported by CONICET doctoral scholarships. N.E. was supported by a FONCyT doctoral fellowship. M.P.A. is a staff researcher from CONICET.

Address correspondence and reprint requests to Dr. Maria Pilar Aoki, Centro de Investigaciones en Bioquímica Clínica e Inmunología–Consejo Nacional de Investigaciones Científicas y Técnicas, Universidad Nacional de Córdoba, Haya de la Torre and Medina Allende, Ciudad Universitaria, Córdoba 5000, Argentina. E-mail address: paoki@fcq.unc.edu.ar

The online version of this article contains supplemental material.

Abbreviations used in this article: ADO, adenosine; APCP, ADO 5′-α,β-methylene-diphosphate; CD73KO, CD73-deficient; CK, total creatine kinase; CK-MB, creatine kinase muscle–brain isoenzyme; dpi, day postinfection; ECG, electrocardiogram; iNOS, inducible NO synthase; M1, classically activated; M2, alternatively activated; Ma, macrophage; ROS, reactive oxygen species.

enhancing the arginase activity and mannose receptor (CD206) expression, to promote wound healing and reduce Th1 response. Moreover, the M2 subset can be also detrimental to the host, leading to tissue fibrosis when their matrix-enhancing activity is not regulated (6). Although Ma can be driven to either M1 or M2 phenotype, the complex in vivo cardiac environment typically produces intermediate phenotypes that coexpress both M1 and M2 markers (7, 8). Nevertheless, some helminth parasite infections induce monocyte recruitment and subsequent expansion of cardiac Ma that become strongly M2-like cells (7), suggesting that myocardial Ma are able to be selectively skewed toward an M2-polarized phenotype in response to Th2-type immunological challenge.

In the setting of Chagas disease, Ma are one of the main infiltrating leukocytes arriving early to myocardium (9), and they remain as an important immune cell population in heart explants from patients with severe advanced chronic Chagas disease (10). Interestingly, selective depletion of Ma causes a significant increment in the number of *T. cruzi* amastigote nests within cardiomyocytes, suggesting a crucial role for Ma in resistance to this infection (11). We have reported that the peak of parasite load is correlated with the peaks of arginase-1 and inducible NO synthase (iNOS) expression in murine *T. cruzi*–infected heart tissue. Moreover, cardiac arginase-1 expression in BALB/c mice is higher and persists for a longer period than in C57BL/6 mice, which exhibits lower myocardial parasite load and is more resistant to the infection (12). Our data clearly indicate that arginase-1, which is induced during the activation of M2 Ma, is associated with parasite growth and susceptibility to infection.

One potential regulatory system deputed to fine-tune immune cell functions is represented by the extracellular adenosine (ADO) level. Postinfection, the influx of immune cells consumes large quantities of oxygen, and ischemic cells rapidly respond to the hypoxic and inflammatory environment by releasing ATP (normally present within cardiomyocytes in millimolar concentrations) (13, 14). Once released, the ATP is converted to ADP/AMP and then to ADO by the ectonucleoside triphosphate diphosphohydrolase-1 (CD39) and the ecto-5'-nucleotidase (CD73), respectively. ADO affects diverse Ma functions, particularly on the M1 subset; it induces: 1) suppression of chemokine production (15); 2) reduction of proinflammatory cytokine production (TNF, IL-1β, IL-6, and IL-12) (16, 17); 3) downregulation of NO production (18); and 4) switching toward the production of anti-inflammatory cytokine IL-10 (16, 17). In addition to these anti-inflammatory effects, CD73 enzymatic activity induces cardiac Ma to adopt an M2-biased phenotype and drives the timely resolution of inflammation (14). Several lines of evidences show that ATP catabolic machinery plays an important role in influencing the outcome of some pathophysiological events (19).

In this study, we focused on the consequences of in vivo manipulation of CD73 activity and its impact on the outcome of Chagas cardiomyopathy. First, we comprehensively studied the kinetic of cardiac Ma phenotypes during the acute and chronic phase of *T. cruzi* infection. We found that under this Th1 stimulus, Ma with M1 phenotype ($CD45^+F4/80^+CD11b^+CD86^+CD206^-$) were early and transiently observed within the myocardium, but Ma were rapidly polarized toward the M2 phenotype ($CD45^+F4/80^+CD11b^+CD86^-CD206^+$), which remained sustained during the acute and chronic phase (90 d postinfection [dpi]). Furthermore, an important Ma subset with both M1 and M2 markers ($CD86^+$ and $CD206^+$) was uniformly observed as the main heart Ma subset throughout the studied period. Interestingly, the temporal pharmacological inhibition of CD73 enzymatic activity induced the shift of cardiac Ma toward a microbicidal phenotype, and decreased the percentage of IL-4– and IL-10–producing $CD4^+$ T lymphocytes, with the concomitant reduction in tissue parasite load and the consequent improvement in the outcome of chronic cardiomyopathy. Summing up, our results demonstrated the key role of ATP metabolic pathway in driving the Ma response to infection and suggest the therapeutic potential of Ma profile manipulation to improve the disease progression at heart level.

Materials and Methods

Ethics statement

All animal experiments were carried out in strict accordance with the recommendations in the *Guide to the Care and Use of Experimental Animals* published by the Canadian Council on Animal Care and approved (Office of Laboratory Animal Welfare, National Institutes of Health, assurance number A5802-01). The Committee on Ethics of Animal Experiments from Centro de Investigaciones en Bioquímica Clínica e Inmunología–Consejo Nacional de Investigaciones Científicas y Técnicas also approved the animal handling and experimental procedures (authorization No. 15-01-44195 and HCD resolution 274/09).

Mice

BALB/c and C57BL/6 mice were purchased at Facultad de Ciencias Veterinarias, Universidad Nacional de La Plata, Argentina. CD73-deficient ($CD73KO\text{-}B6.129S1\text{-}Nt5e^{tm1Lft}/J$) mice were purchased at The Jackson Laboratory. Mice were housed at the Animal Facility of Facultad de Ciencias Químicas, Centro de Investigaciones en Bioquímica Clínica e Inmunología–Consejo Nacional de Investigaciones Científicas y Técnicas, Universidad Nacional de Córdoba.

Experimental infection

Six- to eight-week-old female mice were infected i.p. with 1×10^3 *Trypanosoma cruzi* blood-derived trypomastigotes of Tulahuen strain. Bloodstream trypomastigotes forms were harvested by heart puncture from *T. cruzi*–infected mice at the peak of parasitemia. Parasites were maintained by serial passages from mouse to mouse.

Heart- infiltrating cell isolation

Cardiac leukocyte isolation was performed as described in detail previously (20) with few modifications. Briefly, at indicated time points, infected hearts were perfused with PBS (Life Technologies), weighed, and disaggregated mechanically and enzymatically with 0.2% of trypsin solution (Life Technologies). The digested tissue was gently pressed through a 70-μm cell strainer and washed with PBS. Mononuclear cells were obtained by Ficoll-Hypaque density gradient centrifugation (GE Healthcare). In contrast, when it is indicated, granulocytes and mononuclear cells were isolated from cardiac tissue by a 35% and 70% bilayer Percoll gradient (GE Healthcare). Cell viability was determined by trypan blue exclusion using a Neubauer's chamber. Then, cells were stained for flow cytometry.

Flow cytometry analysis

Cardiac-infiltrating leukocytes were stained using a standard protocol with the following Abs: rat monoclonal anti-mouse CD45 FITC, CD45 allophycocyanin, CD11b allophycocyanin, F4/80 PE, F4/80 PE-Cy7, CD86 allophycocyanin/Cy7, CD206 PE-Cy7, CD3 FITC, CD4 allophycocyanin-Cy7, Ly6G allophycocyanin-Cy7, CD73 PerCP-Cy5.5, and CD39 Biotin plus streptavidin-FITC (eBioscience, BD Pharmingen, and BioLegend). To evaluate the intracellular study, first cardiac mononuclear cells were treated with GolgiStop for 4 h at 37°C, and then cells were surface-labeled as mentioned above. After, samples were fixed and permeabilized with BD Cytofix/Cytoperm and Perm/Wash (BD Biosciences) according to the manufacturer's instruction. Finally, permeabilized cells were incubated with the following Abs: monoclonal anti-mouse IL-4 allophycocyanin, IL-6 FITC, IL-10 allophycocyanin, IL-10 PE-Cy7, IL-17 PE, IFN-γ PerCP-Cy5.5, TNF PerCP-Cy5.5, arginase-1 FITC, or iNOS plus anti-rabbit IgG allophycocyanin (eBioscience, BD Pharmingen, and BioLegend). Oxidation-sensitive dyes DAF-FM DA and DCF DA (10 μmol; Molecular Probes) were used to measure reactive oxygen species (ROS) and NO production, respectively.

TaqMan real-time PCR assay for parasite burden

To determinate the tissue parasitism, genomic DNA was purified from hearts of 4, 14, and 21 dpi using TRIzol reagent and following the manufacturer's instruction. Satellite DNA from *T. cruzi* (GenBank AY520036) was quantified by real-time PCR using specific Custom TaqMan Gene Expression Assay (Applied Biosystems) and employing primer and probe sequences

previously described (21). A sample containing 1 μg genomic DNA was amplified. Abundance of satellite DNA from *T. cruzi* was normalized to GAPDH abundance (TaqMan Rodent GAPDH Control Reagent; Applied Biosystems) and expressed as arbitrary units.

Measurement of chemokine and cytokine

At indicated time points, hearts were perfused and disaggregated mechanically in buffer RIPA. ELISA sandwich was performed for the quantification of MCP-1, IL-17A, IL-4, TGF-β, IL-10, TNF, IL-1β, IL-6, IFN-γ, and IL-12 within the myocardial tissue and in serum. Briefly, ELISA plates were coated with anti-cytokine Abs (BD Pharmingen and e-Bioscience) overnight at 4°C, washed, and blocked with 10% FBS-PBS. Samples were incubated overnight at 4°C. Then, the plates were incubated with biotin anti-cytokine Ab (BD Pharmingen and eBioscience) for 1 h at room temperature. After washing, streptavidin-peroxidase (BD Pharmingen) was added and incubated for 30 min. The reaction was revealed using TMB Substrate Reagent (BD Pharmingen), before being read a 450 nm in a Microplate reader (Bio-Rad). Standard curves were generated using recombinant cytokines (BD Pharmingen and eBioscience). In parallel, total protein concentrations of the heart samples were determined by the Bradford method (Bio-Rad). Data are expressed as the mean of the rate between picograms of cytokine and micrograms of heart total protein.

ADO 5′-α,β-methylene-diphosphate treatment

Infected BALB/c mice were treated i.v. with 20 mg/kg/d ADO 5′-α,β-methylene-diphosphate (APCP) (Sigma-Aldrich) as previously described (22), for 3 consecutive d since 4 dpi. Nontreated infected mice were used as controls. At 7 dpi, cardiac-infiltrating mononuclear cells were isolated and stained for FACS as described above. In other experiments, the myocardium homogenates in RIPA buffer were collected. For parasitemia, blood obtained by cardiac puncture was employed to perform the parasite counting using a Neubauer's chamber.

Electrocardiographic studies and measurement of myocardial damage biomarkers

Electrocardiograms (ECGs) at 90 dpi were performed with an electrocardiograph (model FD-16; Fukuda Denshi) under ketamine hydrochloride (Ketalar 50; Holliday) anesthesia, 10 mg/kg i.p. administration. ECG tracings were obtained with six standard leads (dipolar leads DI, DII, and DIII and unipolar leads aVR, aVL, and aVF), recording at 50 mm/s with amplitude set to give 1 mV/10 mm. In order to follow the progress of the cardiopathy, ECG evaluated parameters were: 1) heart rate (bpm); and 2) modifications in atrioventricular conduction (prolonged PR interval) and ventricular conduction (prolonged QT interval) in milliseconds. Plasma samples were derived to Biocon Laboratory, Córdoba, Argentina, to measure total creatine kinase (CK) and CK muscle–brain isoenzyme (CK-MB) (Bio.System).

Measurement of NO concentration

NO concentration was determined by measuring nitrite levels in cardiac tissue of treated and nontreated infected mice using the Griess reaction (Sigma-Aldrich), as previously described (23). In parallel, the total protein concentrations of the heart samples were determined by the Bradford method (Bio-Rad). Data are expressed as the mean of the rate between nanomoles of NO and micrograms of heart total protein.

Western blot assay

The protein concentration in myocardium homogenate in RIPA buffer was measured by the Bradford method (Bio-Rad). Then, aliquots with equal amounts of protein were separated on SDS-PAGE and electrotransferred to nitrocellulose membranes (Bio-Rad). After being blocked, membranes were incubated with rabbit polyclonal anti-CD39 Biotin Ab (BioLegend). Then, membranes were incubated with streptoavidin-HRP (BD Pharmingen) and reveled using the ECL chemiluminescent system (Amersham Pharmacia Biotech). Finally, they were washed and incubated with rabbit polyclonal anti-actin (Santa Cruz Biotechnology), washed, and revealed with HRP-conjugated anti-rabbit Ab (Sigma-Aldrich). The band intensity for CD39 was semiquantified by densitometric scanning and normalized with respect to actin expression using ImageJ processing software (National Institutes of Health; http://www.rsb.info.nih.gov/ij).

Heart histology and inflammatory index

Paraffin-embedded cardiac tissue-sections obtained from APCP-treated and nontreated infected mice at 90 dpi were subjected to H&E staining. The index of inflammation were scored semiquantitatively on low-power microscopic examination according to distribution and extent of inflammatory cells in epicardium and in myocardium (1+ for a single inflammatory foci, 2+ multiple, nonconfluent foci of inflammatory infiltrate, 3+ for confluent inflammation, and 4+ for diffuse inflammation extended through the section). In addition, the semiquantification of endothelial cell enlargement, perivascular edema, and disrupted and necrotic myocardial fiber were also assessed. The numerical sum for each heart sections (n = 4) represented an estimate of the inflammation index. The slides were photographed in a Nikon Eclipse TE2000-U inverted microscope using a 20× objective (Nikon).

Statistical analysis

To compare different experimental conditions, an ANOVA (two-way or one-way ANOVA) with the Tukey post hoc test was performed. A two-tailed Student t test was used for comparison between two groups. A p value <0.05 was considered significant.

Results

Cardiac Ma exhibited an alternative phenotype early postinfection that predominated throughout the acute and chronic phase

To gain insights into the time course of Ma profiles triggered by *T. cruzi* during the establishment of cardiac infection, we first analyzed the kinetics of Ma subsets within the myocardium of infected BALB/c mice using the gating strategy shown in Fig. 1A. After Ficoll-Hypaque gradient centrifugation, single-cell suspensions from freshly obtained leukocyte-enriched fractions ($CD45^+$) were analyzed for Ma as $F4/80^+CD11b^+$ cells. In the setting of our model, ∼100% of $F4/80^+$ cells were concomitantly positive for CD11b. This myeloid population was further divided based on M1 ($CD86^+$ $CD206^-$) and M2 ($CD86^-CD206^+$) phenotype. Among the Ma with M1 phenotype, the 75.14 ± 3.57% were positive for NO production, whereas the 89.27 ± 10.6% of Ma with the M2 phenotype were positive for arginase-1 expression. We observed that although infiltrating mononuclear cells increased within the myocardium as the acute phase of infection progressed, this immune population dramatically diminished during the chronic phase (90 dpi) (Fig. 1B). These changes were not reflected in cardiac tissue weight because it did not present significant differences at all time points studied (Supplemental Fig. 1A). Among the mononuclear population, Ma were rapidly recruited to the infected heart tissue, but then they progressively decreased, whereas the number of T lymphocytes ($CD3^+$) increased (Fig. 1C). Shortly postinfection (4 dpi), the percentage of Ma with M1 inflammatory phenotype predominated over the M2 Ma subset (Fig. 1D, 1F). Nevertheless, as soon as 7 dpi, the M1 population diminished, whereas Ma with M2 phenotype strongly increased and remained significantly sustained during the acute and chronic phase of the infection. This shift in the percentage of both Ma subsets was also evidenced with the absolute cell number of each subpopulation (Fig. 1E). It is important to stress that although different aspects of the immune response against *T. cruzi* are influenced by the host genetic background (12, 24–26), the same kinetics of Ma profile were observed in the myocardium of infected BALB/c and C57BL/6 mice (L. M. Sanmarco, N. E. Ponce, L. M. Visconti, N. Eberhardt, M. G. Theumer, A. R. Minguez, M. P. Aoki, submitted for publication). These results indicate that cardiac Ma respond to *T. cruzi* infection with an early microbicidal M1 phenotype, but this Ma subtype is rapidly replaced by the M2 anti-inflammatory subtype, which remained as an important subpopulation in infected heart tissue. Hence, throughout the acute and chronic infection, the local milieu promoted mainly the anti-inflammatory and wound-healing Ma profile instead of the antiparasitic subset, likely favoring parasite persistence in cardiac tissue. Notably, Ma with mixed expression of M1/M2 markers ($CD45^+F4/80^+CD11b^+CD86^+CD206^+$), previously described in myocardium, joint, and CNS (7, 8, 27, 28), were the main heart subpopulation

throughout the study period (Fig. 2A). The intracellular staining demonstrated that they coproduced M1- and M2-related cytokines, such as TNF, IL-6, IL-4, and IL-10 (Fig. 2B). Moreover, they also produced the microbicidal effectors NO and ROS (Fig. 2C) and expressed the M2 effector enzyme arginase-1 (Fig. 2D). This mixed population likely allows cellular plasticity and in consequence the fast shift between proinflammatory M1 and wound-healing M2 subset.

Considering that chemokines and cytokines play a central role in the orchestration and timing of the intrinsic cardiac stress response, they are important candidates for regulating the recruitment and local activation of Ma within the myocardium. We therefore analyzed the levels of inflammatory and anti-inflammatory soluble mediators within the cardiac tissue at different times postinfection (Fig. 3). A progressive increment in the levels of the chemokine MCP-1 and an early enhanced production of the inflammatory IL-17A were observed during the infection. Considering that both soluble mediators exert potent chemotactic activity on monocyte/Ma and T lymphocyte as well, these results correlated with the early recruitment of Ma and the later influx of T lymphocytes observed in the kinetic study (Fig. 1C). In agreement, the histological analysis of heart sections showed that local inflammation increased (Supplemental Fig. 1B) together with the rise of mononuclear cell infiltration (Fig. 1B). Although the IL-4 levels remained unchanged, the anti-inflammatory cytokines TGF-β and IL-10 peaked at 14 dpi, consistent with the M2 phenotype predominance over M1 phenotype. In contrast, the levels of proinflammatory Th1 cytokines (TNF, IL-1β, IL-6, IFN-γ, and IL-12) were elevated mainly at early dpi, and they diminished at later times postinfection. In contrast, the same soluble mediators showed a different kinetic in serum (Supplemental Fig. 1F), suggesting that the local but not the systemic microenvironment drives Ma activation profile within the myocardium.

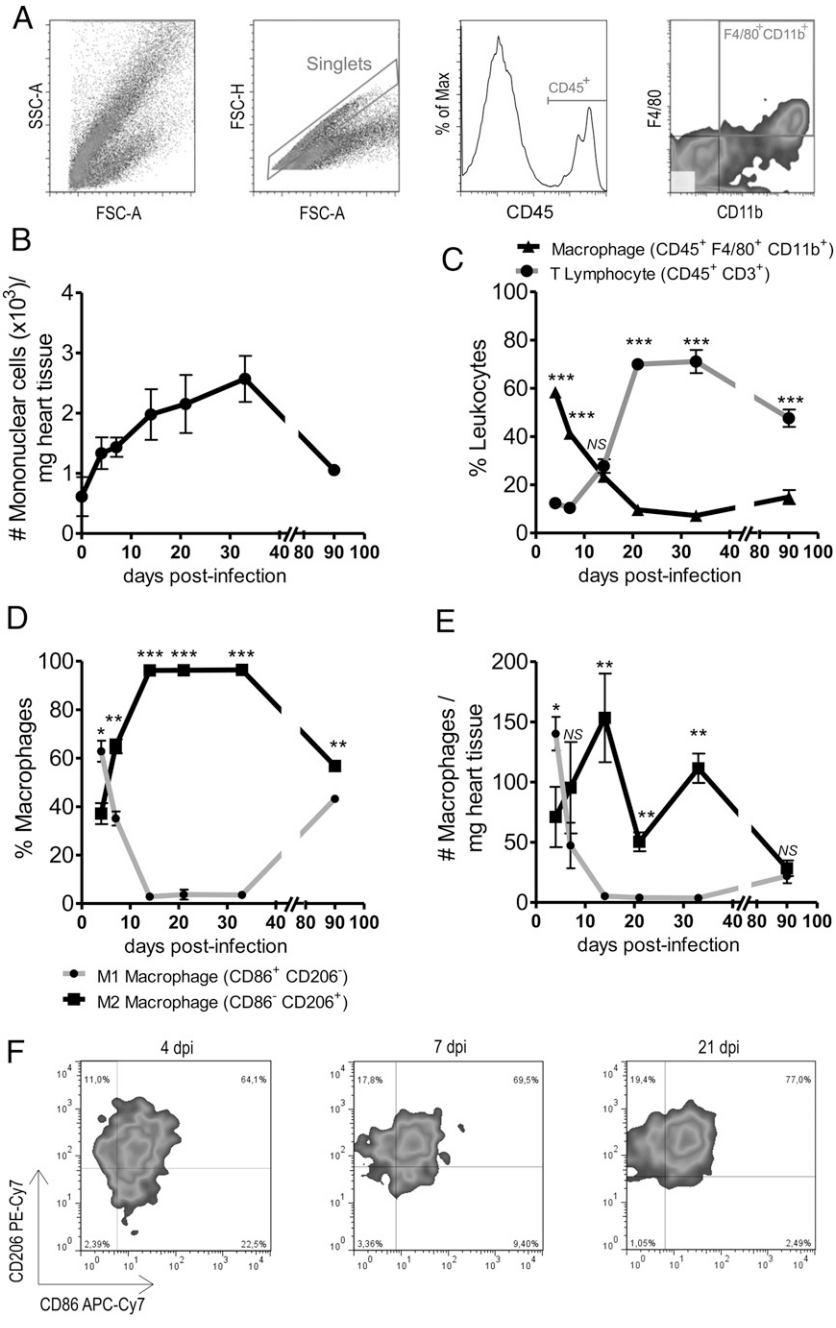

FIGURE 1. Kinetic of cardiac macrophage subsets. (**A**) Flow cytometry gating strategy. First, forward light scatter-height (FSC-H)/forward light scatter-area (FSC-A) dot blots were used to exclude doublets for further study. Mononuclear leukocytes were gated according to their FSC-A and side scatter-area (SSC-A) features and CD45-positive staining. The subpopulations were then evaluated based on the expression of CD206 and CD86 in cells gated on F4/80$^+$CD11b$^+$. (**B**) Number of mononuclear cells per milligram of heart tissue at indicated dpi. (**C**) Percentage of Ma (F4/80$^+$ CD11b$^+$, triangles) and T lymphocytes (CD3$^+$, circles) at different time points. The cells were previously gated on CD45$^+$ cells. Relative percentage (**D**) and number per milligram (**E**) of heart tissue of M1 (CD86$^+$CD206$^-$, circles) and M2 (CD86$^-$CD206$^+$, squares) Ma at indicated dpi, pregated on CD45$^+$F4/80$^+$CD11b$^+$ cells. The percentages of M1 and M2 cells were expressed as the relationship between both single-positive subpopulations. (**F**) Representative dot blots of CD206 expression versus CD86 expression on cardiac Ma population. Results are mean ± SEM (n = 5 mice per each dpi) and represent four independent experiments. *$p < 0.05$, **$p < 0.01$, ***$p < 0.001$.

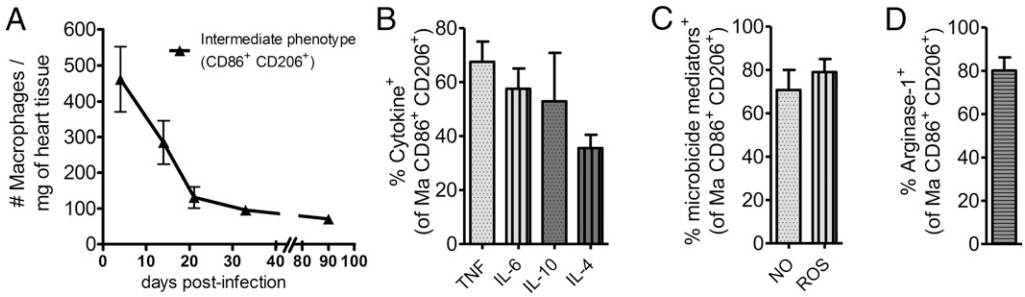

FIGURE 2. Kinetic of cardiac macrophage subset with intermediate phenotype. (**A**) Number of Ma with mixed phenotype ($CD45^+F4/80^+CD11b^+CD86^+CD206^+$) per milligram of heart tissue at indicated dpi. Proportion of Ma with intermediate phenotype positive for intracellular TNF, IL-6, IL-10, IL-4 (**B**), NO, ROS (**C**), and arginase-1 (**D**) expression, analyzed at 14 dpi. Results are mean ± SEM (n = 5 mice per each dpi) and represent two independent experiments.

The inhibition of CD73-mediated ADO production sustained M1 Ma phenotype, reduced the frequency of IL-4– and IL-10–producing $CD4^+$ T cells, and enhanced the inflammatory cytokine milieu in infected myocardium

An impaired microbicidal response during infection has particularly important consequences for myocardial *T. cruzi* persistence, which is the main trigger of the cardiomyopathy. Because one potential regulatory system for local Ma functions is represented by the extracellular ADO levels, we first examined the cell-surface expression of both ectonucleotidases, CD39 and CD73, on cardiac immune cells after *T. cruzi* infection. Recruited Ma, neutrophils, and T lymphocytes expressed CD39 and CD73 (Fig. 4A). There were no differences in CD73 expression between cardiac M1 and M2 Ma subsets (Supplemental Fig. 1C); however, strikingly, a clear selective expression of CD39 and CD73 was observed on resident Ma ($F4/80^{hi}$) population when compared with infiltrating ($F4/80^{low}$) subset (Supplemental Fig. 1D) (29). Moreover, a very low percentage of isolated cardiomyocytes expressed CD39 and CD73 (data not shown). Fig. 4B shows that the CD39 expression in total heart tissue was significantly increased at 21 dpi compared with noninfected control mice. Altogether, these data demonstrate that the enzymatic machinery required to produce ADO from extracellular ATP was present in cardiac leukocytes during the acute infection.

Considering that ADO limits the microbicidal effect of Ma, leading to an increase in the expression of alternative Ma markers, we aimed to lengthen the microbicidal M1 profile in the myocardium through the transient pharmacological inhibition of CD73 enzymatic activity at early times postinfection. Toward this aim, infected BALB/c mice were treated with CD73-specific inhibitor APCP for 3 consecutive d starting at day 4 postinfection, and different parameters were measured at 7 dpi. The APCP treatment increased the number of circulating leukocytes, but it did not modify the proportion of inflammatory ($CD11b^+$ $Ly6C^{hi}$) and resident/patrolling ($CD11b^+Ly6C^{low}$) monocyte subsets (Supplemental Fig. 1E). In myocardium, the amount of mononuclear cells in treated infected mice was also increased compared with nontreated infected control mice (Fig. 5A). This finding was consistent with previously reported results, which demonstrated the key role of the CD73/ADO pathway in the regulation of leukocyte trafficking into inflamed tissue (30). Although there were no significant differences in the percentage of cardiac Ma from total $CD45^+$ cells between treated and nontreated infected mice, the inhibition of CD73 increased the absolute number of this cell type (Fig. 5B). As was expected, in contrast to control mice that presented a sustained biased profile toward M2 Ma phenotype, in APCP-treated mice, the M1 Ma profile predominated over M2 (Fig. 5C). In accordance with these data, preliminary results obtained in

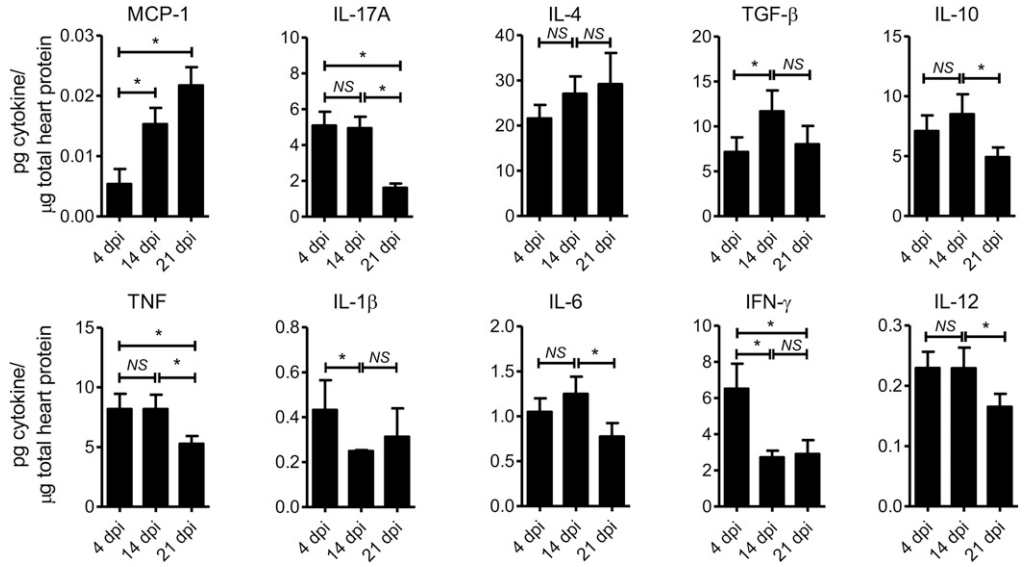

FIGURE 3. Kinetic of chemokine and cytokine levels in the infected myocardium. Levels of MCP-1, IL-17A, IL-4, TGF-β, IL-10, TNF, IL-1β, IL-6, IFN-γ, and IL-12 within myocardial tissue were measured at indicated dpi by ELISA. Results are mean ± SEM (n = 5 mice per each dpi) and represent three independent experiments. *$p < 0.05$.

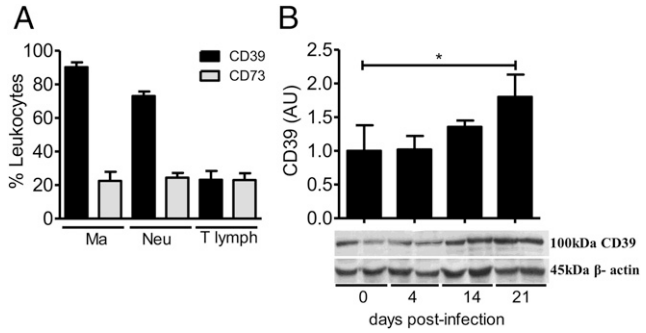

FIGURE 4. CD39 and CD73 expression on cardiac leukocytes and heart tissue during *T. cruzi* infection. (**A**) The percentage of CD39- and CD73-positive cells gated on Ma ($CD45^+F4/80^+CD11b^+Ly6G^-$), neutrophils (Neu: $CD45^+CD11b^+Ly6G^+$), or T lymphocytes (T lymph: $CD45^+CD3^+$) at 4 dpi. (**B**) Western blot analysis of CD39 expression in heart tissue from noninfected and infected mice at indicated time points. The ecto-enzyme expression was normalized with respect to β-actin expression. Data are mean ± SEM of two independent experiments ($n = 4$ mice per each dpi). $^*p < 0.05$. AU, arbitrary units.

CD73KO mice showed that cardiac M1 Ma predominated over M2 Ma phenotype at 7 dpi, in contrast to the M2 predominance observed in control infected C57BL/6 mice at this time point (Fig. 5D). Therefore, supporting our hypothesis, these findings demonstrated that the absence of CD73-generated ADO potentiated the Ma microbicidal phenotype.

Given the important role of T cells in orchestrating the immune response and considering that different T cell subsets express CD73, we further focused on the effect of transient APCP treatment on cardiac $CD4^+$ T lymphocytes. We found that the inhibition of CD73 activity did not modify the percentage of cardiac $CD4^+$ T lymphocytes but increased the absolute number of this T cell population (Fig. 5E). In line with the shift in M1/M2 rate induced by APCP administration, the treatment significantly diminished the percentages of IL-$4^+CD3^+CD4^+$ cells as well as IL-10^+CD3^+ $CD4^+$ cells, whereas the proportion of $CD3^+CD4^+$ lymphocytes positive for IFN-γ did not exhibit changes (Fig. 5F). In addition, the treatment induced a reduction in IL-17–producing T cell subset. These results suggest that inhibition of CD73 enzymatic activity modified the cytokine production by cardiac $CD4^+$ T cells.

In order to determine the impact of the transient inhibition of CD73 activity on the local chemokine and cytokine production, we measured their levels within the heart tissue at 7 dpi (Fig. 5H). Supporting the increment in the mononuclear cell infiltration observed in CD73-inhibited mice, the amount of cardiac MCP-1 was significantly enhanced compared with control nontreated mice. In parallel with the M1 population predominance caused by APCP treatment, the inflammatory cytokines TNF, IL-1β, and IL-6 were significantly increased compared with the measured levels in nontreated mice at this time point. No changes were observed in Th1-related cytokine IFN-γ and IL-12 levels. Despite the decrease on the M2 Ma population, the levels of IL-4 significantly increased, whereas IL-17, TGF-β, and IL-10 production were not

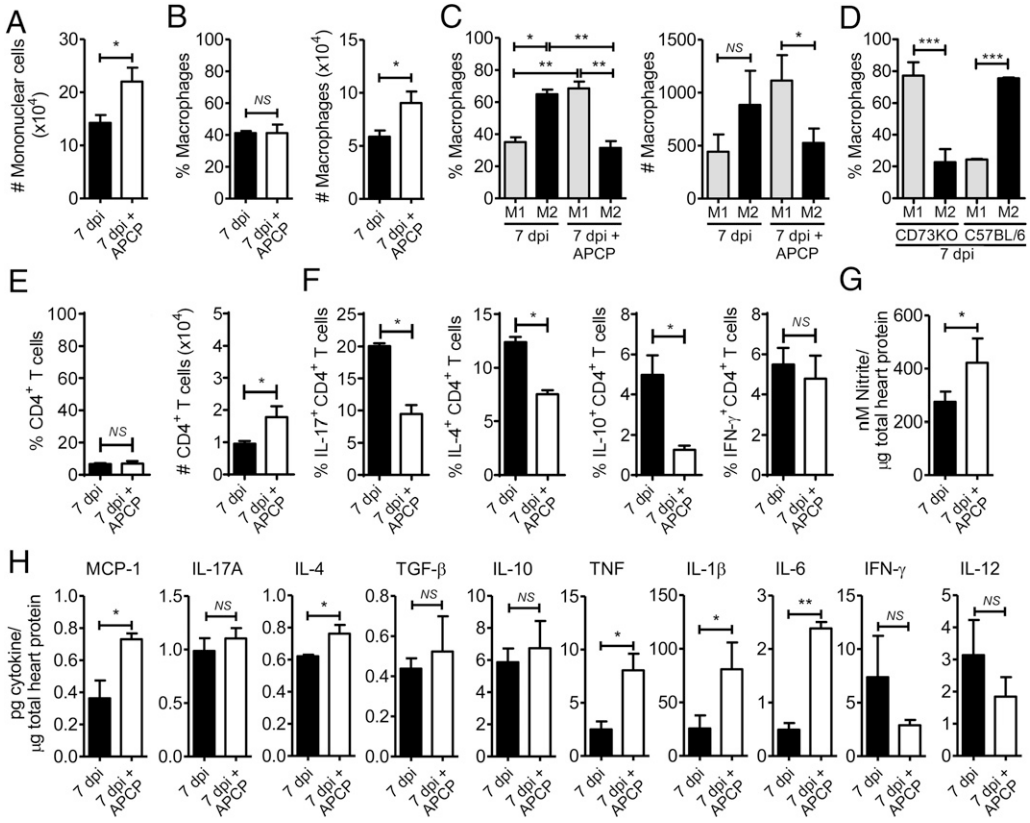

FIGURE 5. APCP treatment induced the shift toward M1 Ma phenotype in infected heart tissue. (**A**) Number of cardiac mononuclear cells at 7 dpi. (**B**) Percentage and number of cardiac Ma ($F4/80^+CD11b^+$) from APCP-treated and nontreated mice at 7 dpi. (**C**) Relative percentage and number of M1 and M2 subsets in treated and nontreated myocardium. (**D**) Relative percentage of M1 and M2 subsets in CD73KO and C57BL/6 mice at 7 dpi. (**E**) Percentage and number of cardiac T lymphocytes ($CD3^+$ $CD4^+$) from APCP-treated and nontreated mice at 7 dpi, pregated on $CD45^+$ cells. (**F**) Proportion of cardiac IL-17, IL-4, IL-10, and IFN-γ–producing $CD4^+$ T lymphocytes from treated and nontreated mice at 7 dpi, pregated on $CD45^+CD3^+$ cells. Nitrite (**G**), chemokine, and cytokine levels (**H**) within myocardial tissue. The results are mean ± SEM ($n = 6$ mice per each dpi) of a representative assay of at least two independent experiments. $^*p < 0.05$, $^{**}p < 0.01$, $^{***}p < 0.001$.

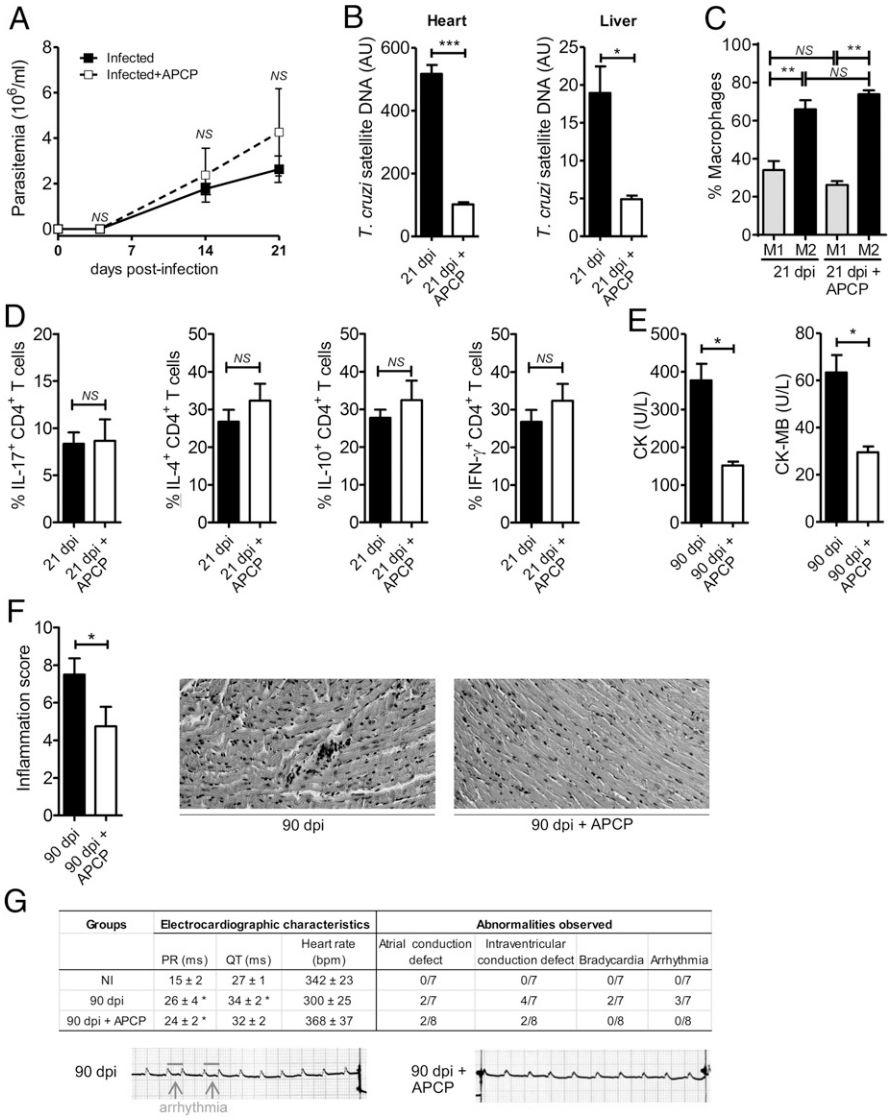

Groups	Electrocardiographic characteristics			Abnormalities observed			
	PR (ms)	QT (ms)	Heart rate (bpm)	Atrial conduction defect	Intraventricular conduction defect	Bradycardia	Arrhythmia
NI	15 ± 2	27 ± 1	342 ± 23	0/7	0/7	0/7	0/7
90 dpi	26 ± 4 *	34 ± 2 *	300 ± 25	2/7	4/7	2/7	3/7
90 dpi + APCP	24 ± 2 *	32 ± 2	368 ± 37	2/8	2/8	0/8	0/8

FIGURE 6. CD73 inhibition ameliorated the outcome of experimental Chagas cardiomyopathy. (**A**) Parasitemia curve of APCP-treated and nontreated mice ($n = 8$ per group). (**B**) Quantitative assessment of cardiac and hepatic parasite load by real-time PCR using TaqMan probes ($n = 4$ per group) at 21 dpi. (**C**) Relative percentage of M1 and M2 subsets in treated and nontreated myocardium at 21 dpi. (**D**) Proportion of cardiac IL-17, IL-4, IL-10, and IFN-γ–producing $CD4^+$ T lymphocytes from treated and nontreated mice at 21 dpi. (**E**) Total CK and CK-MB activities in treated and nontreated serum at 90 dpi ($n = 8$ per group). The results are mean ± SEM of at least two independent experiments. $*p < 0.05$, $**p < 0.01$, $***p < 0.001$. (**F**) Inflammatory score of APCP-treated and nontreated myocardium obtained at 90 dpi. Representative images of treated and nontreated myocardial sections at 90 dpi are shown (original magnification ×200). (**G**) ECG parameters and abnormalities observed in noninfected mice (NI; $n = 7$), control mice ($n = 7$), and APCP-treated infected mice ($n = 8$) at 90 dpi. ECG parameters were evaluated using the following standard criteria: the variation of the PR and QT intervals measured in milliseconds and heart rate monitored by beats per minute. Values are mean ± SEM of two independent experiments. Bottom panel, Representative ECG tracing from each infected group. Arrows point to arrhythmia. $*p < 0.05$ versus NI.

modified by CD73 inhibition. In contrast, the levels of NO increased in the myocardium of CD73-inhibited mice (Fig. 5G), in agreement with the observed promotion of M1 phenotype. Overall, CD73 inhibition not only modifies Ma phenotype and $CD4^+$ T lymphocyte cytokine production but also shifts infected heart tissue environment toward an inflammatory milieu.

CD73 inhibition ameliorated the outcome of experimental Chagas cardiomyopathy

Although there were no differences in parasitemia between treated and nontreated group of animals (Fig. 6A), the treatment induced a significant reduction of parasite burden of heart tissue and liver at 21 dpi (Fig. 6B). At this time point, there were no differences in cardiac M1/M2 rate or $CD4^+$ T lymphocyte percentages between APCP-treated and nontreated infected mice (Fig. 6C, 6D), suggesting that the diminution of tissue parasite load induced by APCP was a result of earlier changes in the local immune response against *T. cruzi*. In line with the improvement in parasite replication control, a significant diminution of both serum CK and CK-MB activity was observed during the chronic stage of infection (90 dpi) in APCP-treated mice compared with control nontreated mice (Fig. 6E). Total serum CK and CK-MB activity have long been the standard biochemical markers for nonspecific tissue damage and specific myocardial injury, respectively. Accordingly, the ECGs of APCP-treated mice were improved compared with control mice (Fig. 6G). The ECG characteristics showed no differences in the heart rate among the groups. However, significant alterations in the PR intervals were measured in both APCP-treated and nontreated infected mice, indicating slower transmission in electrical impulses atrioventricular, likely due to the inflammatory process. In contrast, nontreated group presented a significant prolongation in the QT intervals, suggesting intraventricular conduction blockages; meanwhile, this abnormality was not observed in the APCP-treated group. Moreover, none of the CD73 inhibited-mice presented bradycardias or arrhythmias, in contrast to nontreated mice, which exhibited these abnormalities in the ECG tracing. In agreement, the treatment induced a diminution in cardiac inflammatory score (Fig. 6F), evidenced by several disrupted myocytes, multifocal inflammatory foci in myocardium, and strong infiltrate in the epicardium.

Summing up, the described results clearly revealed that APCP treatment induces the polarization of cardiac Ma toward microbicidal M1 profile, with a concomitant decrease in cardiac parasite load and in consequence improve the progression of Chagas cardiomyopathy. Therefore, the transient in vivo targeting of CD73 enzymatic activity may be a strategy to manipulate cardiac Ma activation state and could provide a gateway to new therapies at heart level.

Discussion

The present study demonstrates that cardiac Ma polarization during *T. cruzi* infection is strongly influenced by the products of extracellular ATP metabolism and that the manipulation of this pathway could provide new approaches to reduce cardiac pathology in infected hearts. After a comprehensive analysis of the kinetic of Ma subpopulations within infected myocardium, we found that M1 phenotype dominated only at short times postinfection (4 dpi), but then the M2 subset rapidly increased and predominated throughout the acute and chronic phase. The shift in M1/M2 rate observed may provide protection against overwhelming uncontrolled cardiac inflammation; however, the switch toward M2 profile can promote the parasite survival, which has evolved strategies to interfere with M1 activation and its microbicidal function (31, 32). Considering that M1 Ma are responsible for resistance against *T. cruzi* through ROS and NO production and that the peak of parasitemia is reached at 18 dpi in the BALB/c infection model (24, 33, 34), we hypothesize that the sudden shift of M1 profile toward M2 subset at 7 dpi is too early, and, in consequence, the M1 influence is not enough to fight the parasite located into the myocardium. To test this hypothesis, we pharmacologically interrupted the ATP metabolism pathway, a potential regulatory system that could promote the switch from M1 to M2 phenotype via ADO downstream effect.

Extracellular ATP and ADO are two well-studied damage-associated molecular patterns, which initiate and modulate the immune response against pathogens after binding to purinergic receptors. ATP is normally present within cardiomyocytes in millimolar concentrations, and it is secreted in response to stress, such as hypoxia, or after TLR activation. Once in the extracellular milieu, ATP is rapidly converted into ADO via CD39 and CD73-mediated hydrolysis (35). It has been described that ADO induces cardiac Ma to adopt an M2-biased phenotype and drives the timely resolution of postinfarction inflammation (14). Moreover, CD39 and CD73 enzymatic activities exert cardioprotection during myocardial infarction and in ischemic-reperfusion study models (13, 36, 37). The rate-limiting enzyme in ADO generation is CD73 (22), which is expressed on different cell types. Regarding M1 and M2 Ma, both in vitro–polarized populations express CD39 and CD73 as well as most of ATP and ADO receptors (38). In the current study, we found that cardiac Ma, neutrophils, and T lymphocytes expressed CD39 and CD73 during the immune response against *T. cruzi*. Intriguingly, we found that CD73 was selectively expressed on resident Ma, whereas low levels were detected on the infiltrating subpopulation, suggesting that both cardiac Ma subsets could provide a differential contribution to the ATP metabolism. In contrast, in agreement with previous reports (13, 39), we found that a very low percentage of isolated cardiomyocytes expressed CD39 or CD73, suggesting that they do not significantly contribute to the local extracellular ADO levels during *T. cruzi* infection.

The transient administration of a specific competitive CD73 activity inhibitor APCP, during the early acute phase of *T. cruzi* murine infection, increased the amount of leukocytes in heart tissue, in agreement with the reported key role of CD73 in the regulation of leukocyte migration (30). The rise in cardiac Ma was at the expense of a substantive increase in monocyte-derived Ma ($CD11b^+F4/80^{low}$) influx; meanwhile, the number of cardiac-resident Ma ($CD11b^+F4/80^{hi}$) did not exhibit any change compared with infected nontreated animal (data not shown). Regarding the impact on cardiac Ma phenotype, the pharmacological inhibition of CD73 enhanced the frequency and number of classically activated Ma over alternatively activated subset, shifting the M1/M2 ratio observed in nontreated infected mice. These data are consistent with prior studies that have established ADO as a regulator of classical Ma activation and function, including suppression of proinflammatory cytokine and chemokine production and reduction of iNOS activity. In contrast, extracellular ATP promotes M1 features such as ROS, iNOS expression/NO production, inflammasome activation/IL-1β production, proinflammatory cytokine release, and induction of Ma death by necrosis and/or apoptosis (40–42). Accordingly, we observed that APCP treatment induced a significant increment of cardiac M1-related cytokines (IL-1β, IL-6, and TNF) and NO production. The increment in the number of cardiac M1 Ma and the increased NO levels are key factors for *T. cruzi* clearance and consistent with the significantly lower cardiac parasite load observed in APCP-treated animals. Surprisingly, APCP administration increased the cardiac levels of IL-4, although this Th2-related cytokine was unable to maintain the M2 phenotype or counteract the Th1/M1 response. It is likely that other IL-4–producing cells, such as type 2 innate lymphoid cells or eosinophils, could be responsible for the increased levels of this cytokine in treated myocardium. Regarding the increased levels of IL-6 detected in APCP-treated hearts, it is important to stress that this pleiotropic cytokine is a cardioprotective factor. In this sense, we have reported that IL-6 is secreted by cardiomyocytes after *T. cruzi* recognition, and it acts as a key survival factor for these target cells during the infection (43–45).

Regulatory T cells can profoundly affect macrophage activation state and functions. A key mechanism by which $Foxp3^+CD4^+$ regulatory T subset and, mainly, type 1 regulatory T (Tr1) cells control immune response and maintain tissue tolerance is through the secretion of anti-inflammatory cytokines, such as IL-10. In accordance with the shift observed on M1/M2 rate after APCP treatment at 7 dpi, we observed a significant reduction in IL-10–producing $CD4^+$ cardiac T cells compared with nontreated mice. Moreover, although APCP treatment did not modify IFN-γ–producing $CD4^+$ T cells, it diminished the percentages of cardiac IL-4–producing T cells (a key cytokine that promote M2 profile). These results suggest that T cell compartment is also modulated by the transient inhibition of CD73 enzymatic activity.

The immunological events that take place during acute phase influence the outcome of chronic disease. In accord, consistent with the lower parasite load observed in treated heart tissue during the acute phase; the serum levels of CK-MB (biochemical marker of myocardial damage) but also of total CK significantly diminished during the chronic phase (90 dpi), suggesting a potential protective role for APCP treatment over other tissues in addition to myocardium. In line with this, there was an improvement in the ECG of CD73-inhibited animals evidenced by the absence of alterations in the frequency of contractions and a reduction in the number of mice that exhibited intraventricular electrical conduction alterations compared with nontreated infected mice. The main arrhythmogenic substrates in Chagas individuals are necrotic and fibrotic lesions caused by cardiac inflammatory reactions. These processes damage the intercellular junctions that are associated with changes in electrical potential and compromise stimulus conduction between cells. In accord with our results, APCP-treated mice showed significant diminution in the myocardial inflammatory score. Summing up, our results clearly suggest that an earlier control of parasite replication at heart level will favorably impact on the progression of Chagas disease.

Regarding the ectonucleotidase activity from pathogenic agents, it has been recognized as an important virulence factor (46). In this sense, the ecto-nucleoside-triphosphate-diphosphohydrolase, homolog to CD39 family enzymes, is localized on the external surface of all biological stages of *T. cruzi*, and it has been proposed as new chemotherapy target to block the infection (47). Moreover, the infective form (trypomastigote) presents the highest

ATP hydrolysis rate, and its enzymatic activity increases in vitro cell infection and parasitemia in a murine model of Chagas disease (47). However, there are no reports about the effect of APCP in parasite ectonucleotidases. We rule out a potential direct parasiticidal effect of APCP based on the fact that there were no differences in the parasitemia between treated and nontreated mice. However, it is plausible to think that changes in the availability of extracellular ATP and its metabolites may be playing a role in the parasite biology. Further characterization of ectonucleotidases from *T. cruzi* and its purinergic signaling and biology are necessary.

Although it is generally accepted that Ma are phenotypically plastic cells highly influenced by the microenvironment, it remains unclear if their activation states are stable or transient resulting in complex, even mixed phenotypes. Published data have shown the presence of Ma with intermediate phenotype in human CNS (28) and in murine heart tissue after acute myocardial infarction (8) and after a Th2 immunologic challenge (7). In the current study, we found that a subset with a mixed phenotype was the main heart population during all time points studied. About 80% of double-positive Ma were positive for arginase-1 (M2 effector enzyme), NO, and ROS (M1 effector metabolites) expression. The molecular networks orchestrating this mixed phenotype require further exploration. However, considering the poor regenerative capacity of cardiomyocytes and neurons, it is plausible to think that it would be catastrophic for the heart and the CNS to be infiltrated by highly polarized Ma populations.

Taken together, our results demonstrate that the temporal inhibition of CD73 activity prevents the M1 to M2 shift, diminishing the IL-4– and IL-10–producing $CD4^+$ T cells and enhancing the production of NO and proinflammatory cytokines within infected myocardium. The enhanced cardiac antiparasite immune response induced by APCP was evidenced by the substantial reduction of parasite load in parasite target tissues during the acute phase. As a direct consequence, there was an improvement in the outcome of the cardiomyopathy. This work highlights that immunomodulatory therapies focused in the purinergic system could provide a gateway to new therapeutic strategies at the heart level.

Acknowledgments

We thank Dr. María Florencia Harman and Dr. María Cristina Pistoresi-Palencia for the donation of anti-arginase-1 FITC, Dr. Jimena Tosello Boari, Alejandra Romero, Pilar Crespo, Paula Abadie, Carolina Florit, Victoria Blanco, Diego Lutti, and Fabricio Navarro for skillful technical assistance, Dr. Fabio M. Cerbán and Dr. Cinthia C. Stempin for critical revision of the manuscript, and Mabel Enriquez-Algeciras (native speaker) for English grammar revision.

Disclosures

The authors have no financial conflicts of interest.

References

1. World Health Organization. 2015. Chagas disease (American trypanosomiasis). Fact sheet 340. Available at: http://www.who.int/mediacentre/factsheets/fs340/en/. Accessed June 1, 2016.
2. Bonney, K. M., and D. M. Engman. 2008. Chagas heart disease pathogenesis: one mechanism or many? *Curr. Mol. Med.* 8: 510–518.
3. Viotti, R., B. Alarcón de Noya, T. Araujo-Jorge, M. J. Grijalva, F. Guhl, M. C. López, J. M. Ramsey, I. Ribeiro, A. G. Schijman, S. Sosa-Estani, et al; Latin American Network for Chagas Disease, NHEPACHA. 2014. Towards a paradigm shift in the treatment of chronic Chagas disease. *Antimicrob. Agents Chemother.* 58: 635–639.
4. Brener, Z., and R. T. Gazzinelli. 1997. Immunological control of *Trypanosoma cruzi* infection and pathogenesis of Chagas' disease. *Int. Arch. Allergy Immunol.* 114: 103–110.
5. Mosser, D. M., and J. P. Edwards. 2008. Exploring the full spectrum of macrophage activation. *Nat. Rev. Immunol.* 8: 958–969.
6. Tidball, J. G., and S. A. Villalta. 2010. Regulatory interactions between muscle and the immune system during muscle regeneration. *Am. J. Physiol. Regul. Integr. Comp. Physiol.* 298: R1173–R1187.
7. Mylonas, K. J., S. J. Jenkins, R. F. Castellan, D. Ruckerl, K. McGregor, A. T. Phythian-Adams, J. P. Hewitson, S. M. Campbell, A. S. MacDonald, J. E. Allen, and G. A. Gray. 2015. The adult murine heart has a sparse, phagocytically active macrophage population that expands through monocyte recruitment and adopts an 'M2' phenotype in response to Th2 immunologic challenge. *Immunobiology* 220: 924–933.
8. Yan, X., A. Anzai, Y. Katsumata, T. Matsuhashi, K. Ito, J. Endo, T. Yamamoto, A. Takeshima, K. Shinmura, W. Shen, et al. 2013. Temporal dynamics of cardiac immune cell accumulation following acute myocardial infarction. *J. Mol. Cell. Cardiol.* 62: 24–35.
9. Melo, R. C. 2009. Acute heart inflammation: ultrastructural and functional aspects of macrophages elicited by *Trypanosoma cruzi* infection. *J. Cell. Mol. Med.* 13: 279–294.
10. Argüello, R. J., C. Vigliano, P. Cabeza-Meckert, R. Viotti, F. Garelli, L. E. Favaloro, R. R. Favaloro, R. Laguens, and S. A. Laucella. 2014. Presence of antigen-experienced T cells with low grade of differentiation and proliferative potential in chronic Chagas disease myocarditis. *PLoS Negl. Trop. Dis.* 8: e2989.
11. Melo, R. C., and C. R. Machado. 2001. *Trypanosoma cruzi*: peripheral blood monocytes and heart macrophages in the resistance to acute experimental infection in rats. *Exp. Parasitol.* 97: 15–23.
12. Cuervo, H., M. A. Pineda, M. P. Aoki, S. Gea, M. Fresno, and N. Gironès. 2008. Inducible nitric oxide synthase and arginase expression in heart tissue during acute *Trypanosoma cruzi* infection in mice: arginase I is expressed in infiltrating CD68+ macrophages. *J. Infect. Dis.* 197: 1772–1782.
13. Bönner, F., N. Borg, S. Burghoff, and J. Schrader. 2012. Resident cardiac immune cells and expression of the ectonucleotidase enzymes CD39 and CD73 after ischemic injury. *PLoS One* 7: e34730.
14. Bönner, F., N. Borg, C. Jacoby, S. Temme, Z. Ding, U. Flögel, and J. Schrader. 2013. Ecto-5′-nucleotidase on immune cells protects from adverse cardiac remodeling. *Circ. Res.* 113: 301–312.
15. Szabó, C., G. S. Scott, L. Virág, G. Egnaczyk, A. L. Salzman, T. P. Shanley, and G. Haskó. 1998. Suppression of macrophage inflammatory protein (MIP)-1alpha production and collagen-induced arthritis by adenosine receptor agonists. *Br. J. Pharmacol.* 125: 379–387.
16. Németh, Z. H., C. S. Lutz, B. Csóka, E. A. Deitch, S. J. Leibovich, W. C. Gause, M. Tone, P. Pacher, E. S. Vizi, and G. Haskó. 2005. Adenosine augments IL-10 production by macrophages through an A2B receptor-mediated posttranscriptional mechanism. *J. Immunol.* 175: 8260–8270.
17. Cohen, H. B., K. T. Briggs, J. P. Marino, K. Ravid, S. C. Robson, and D. M. Mosser. 2013. TLR stimulation initiates a CD39-based autoregulatory mechanism that limits macrophage inflammatory responses. *Blood* 122: 1935–1945.
18. Haskó, G., C. Szabó, Z. H. Németh, V. Kvetan, S. M. Pastores, and E. S. Vizi. 1996. Adenosine receptor agonists differentially regulate IL-10, TNF-alpha, and nitric oxide production in RAW 264.7 macrophages and in endotoxemic mice. *J. Immunol.* 157: 4634–4640.
19. Antonioli, L., P. Pacher, E. S. Vizi, and G. Haskó. 2013. CD39 and CD73 in immunity and inflammation. *Trends Mol. Med.* 19: 355–367.
20. Pinto, A. R., A. Chandran, N. A. Rosenthal, and J. W. Godwin. 2013. Isolation and analysis of single cells from the mouse heart. *J. Immunol. Methods* 393: 74–80.
21. Piron, M., R. Fisa, N. Casamitjana, P. López-Chejade, L. Puig, M. Vergés, J. Gascón, J. Gómez i Prat, M. Portús, and S. Sauleda. 2007. Development of a real-time PCR assay for *Trypanosoma cruzi* detection in blood samples. *Acta Trop.* 103: 195–200.
22. Forte, G., R. Sorrentino, A. Montinaro, A. Luciano, I. M. Adcock, P. Maiolino, C. Arra, C. Cicala, A. Pinto, and S. Morello. 2012. Inhibition of CD73 improves B cell-mediated anti-tumor immunity in a mouse model of melanoma. *J. Immunol.* 189: 2226–2233.
23. Green, L. C., S. R. Tannenbaum, and P. Goldman. 1981. Nitrate synthesis in the germfree and conventional rat. *Science* 212: 56–58.
24. Carrera-Silva, E. A., R. C. Cano, N. Guiñazú, M. P. Aoki, A. Pellegrini, and S. Gea. 2008. TLR2, TLR4 and TLR9 are differentially modulated in liver lethally injured from BALB/c and C57BL/6 mice during *Trypanosoma cruzi* acute infection. *Mol. Immunol.* 45: 3580–3588.
25. Arocena, A. R., L. I. Onofrio, A. V. Pellegrini, A. E. Carrera Silva, A. Paroli, R. C. Cano, M. P. Aoki, and S. Gea. 2014. Myeloid-derived suppressor cells are key players in the resolution of inflammation during a model of acute infection. *Eur. J. Immunol.* 44: 184–194.
26. Pellegrini, A., N. Guiñazú, M. P. Aoki, I. C. Calero, E. A. Carrera-Silva, N. Girones, M. Fresno, and S. Gea. 2007. Spleen B cells from BALB/c are more prone to activation than spleen B cells from C57BL/6 mice during a secondary immune response to cruzipain. *Int. Immunol.* 19: 1395–1402.
27. Klein-Wieringa, I. R., M. Kloppenburg, Y. M. Bastiaansen-Jenniskens, E. Yusuf, J. C. Kwekkeboom, H. El-Bannoudi, R. G. Nelissen, A. Zuurmond, V. Stojanovic-Susulic, G. J. Van Osch, et al. 2011. The infrapatellar fat pad of patients with osteoarthritis has an inflammatory phenotype. *Ann. Rheum. Dis.* 70: 851–857.
28. Vogel, D. Y., E. J. Vereyken, J. E. Glim, P. D. Heijnen, M. Moeton, P. van der Valk, S. Amor, C. E. Teunissen, J. van Horssen, and C. D. Dijkstra. 2013. Macrophages in inflammatory multiple sclerosis lesions have an intermediate activation status. *J. Neuroinflammation* 10: 35.
29. Davies, L. C., M. Rosas, S. J. Jenkins, C. T. Liao, M. J. Scurr, F. Brombacher, D. J. Fraser, J. E. Allen, S. A. Jones, and P. R. Taylor. 2013. Distinct bone marrow-derived and tissue-resident macrophage lineages proliferate at key stages during inflammation. *Nat. Commun.* 4: 1886.

30. Salmi, M., and S. Jalkanen. 2005. Cell-surface enzymes in control of leukocyte trafficking. *Nat. Rev. Immunol.* 5: 760–771.
31. Stempin, C. C., V. V. Garrido, L. R. Dulgerian, and F. M. Cerbán. 2008. Cruzipain and SP600125 induce p38 activation, alter NO/arginase balance and favor the survival of *Trypanosoma cruzi* in macrophages. *Acta Trop.* 106: 119–127.
32. Giordanengo, L., N. Guiñazú, C. Stempin, R. Fretes, F. Cerbán, and S. Gea. 2002. Cruzipain, a major *Trypanosoma cruzi* antigen, conditions the host immune response in favor of parasite. *Eur. J. Immunol.* 32: 1003–1011.
33. Alvarez, M. N., G. Peluffo, L. Piacenza, and R. Radi. 2011. Intraphagosomal peroxynitrite as a macrophage-derived cytotoxin against internalized *Trypanosoma cruzi*: consequences for oxidative killing and role of microbial peroxiredoxins in infectivity. *J. Biol. Chem.* 286: 6627–6640.
34. Silva, J. S., G. N. Vespa, M. A. Cardoso, J. C. Aliberti, and F. Q. Cunha. 1995. Tumor necrosis factor alpha mediates resistance to *Trypanosoma cruzi* infection in mice by inducing nitric oxide production in infected gamma interferon-activated macrophages. *Infect. Immun.* 63: 4862–4867.
35. Junger, W. G. 2011. Immune cell regulation by autocrine purinergic signalling. *Nat. Rev. Immunol.* 11: 201–212.
36. Eltzschig, H. K., D. Köhler, T. Eckle, T. Kong, S. C. Robson, and S. P. Colgan. 2009. Central role of Sp1-regulated CD39 in hypoxia/ischemia protection. *Blood* 113: 224–232.
37. Cai, M., Z. M. Huttinger, H. He, W. Zhang, F. Li, L. A. Goodman, D. G. Wheeler, L. J. Druhan, J. L. Zweier, K. M. Dwyer, et al. 2011. Transgenic over expression of ectonucleotide triphosphate diphosphohydrolase-1 protects against murine myocardial ischemic injury. *J. Mol. Cell. Cardiol.* 51: 927–935.
38. Zanin, R. F., E. Braganhol, L. S. Bergamin, L. F. Campesato, A. Z. Filho, J. C. Moreira, F. B. Morrone, J. Sévigny, M. R. Schetinger, A. T. de Souza Wyse, and A. M. Battastini. 2012. Differential macrophage activation alters the expression profile of NTPDase and ecto-5′-nucleotidase. *PLoS One* 7: e31205.
39. Eckle, T., T. Krahn, A. Grenz, D. Köhler, M. Mittelbronn, C. Ledent, M. A. Jacobson, H. Osswald, L. F. Thompson, K. Unertl, and H. K. Eltzschig. 2007. Cardioprotection by ecto-5′-nucleotidase (CD73) and A2B adenosine receptors. *Circulation* 115: 1581–1590.
40. Cruz, C. M., A. Rinna, H. J. Forman, A. L. Ventura, P. M. Persechini, and D. M. Ojcius. 2007. ATP activates a reactive oxygen species-dependent oxidative stress response and secretion of proinflammatory cytokines in macrophages. *J. Biol. Chem.* 282: 2871–2879.
41. Pelegrin, P., and A. Surprenant. 2006. Pannexin-1 mediates large pore formation and interleukin-1beta release by the ATP-gated P2X7 receptor. *EMBO J.* 25: 5071–5082.
42. Coutinho-Silva, R., C. Monteiro da Cruz, P. M. Persechini, and D. M. Ojcius. 2007. The role of P2 receptors in controlling infections by intracellular pathogens. *Purinergic Signal.* 3: 83–90.
43. Ponce, N. E., R. C. Cano, E. A. Carrera-Silva, A. P. Lima, S. Gea, and M. P. Aoki. 2012. Toll-like receptor-2 and interleukin-6 mediate cardiomyocyte protection from apoptosis during *Trypanosoma cruzi* murine infection. *Med. Microbiol. Immunol. (Berl.)* 201: 145–155.
44. Ponce, N. E., E. A. Carrera-Silva, A. V. Pellegrini, S. I. Cazorla, E. L. Malchiodi, A. P. Lima, S. Gea, and M. P. Aoki. 2013. *Trypanosoma cruzi*, the causative agent of Chagas disease, modulates interleukin-6-induced STAT3 phosphorylation via gp130 cleavage in different host cells. *Biochim. Biophys. Acta* 1832: 485–494.
45. Aoki, M. P., N. L. Guiñazú, A. V. Pellegrini, T. Gotoh, D. T. Masih, and S. Gea. 2004. Cruzipain, a major *Trypanosoma cruzi* antigen, promotes arginase-2 expression and survival of neonatal mouse cardiomyocytes. *Am. J. Physiol. Cell Physiol.* 286: C206–C212.
46. Berrêdo-Pinho, M., C. E. Peres-Sampaio, P. P. Chrispim, R. Belmont-Firpo, A. P. Lemos, A. Martiny, M. A. Vannier-Santos, and J. R. Meyer-Fernandes. 2001. A Mg-dependent ecto-ATPase in *Leishmania* amazonensis and its possible role in adenosine acquisition and virulence. *Arch. Biochem. Biophys.* 391: 16–24.
47. Santos, R. F., M. A. Pôssa, M. S. Bastos, P. M. Guedes, M. R. Almeida, R. Demarco, S. Verjovski-Almeida, M. T. Bahia, and J. L. Fietto. 2009. Influence of Ecto-nucleoside triphosphate diphosphohydrolase activity on *Trypanosoma cruzi* infectivity and virulence. *PLoS Negl. Trop. Dis.* 3: e387.